Protein Engineering, Design & Selection, 2016, vol. 29 no. 3, pp. 105–115
doi: 10.1093/protein/gzv065
Advance Access Publication Date: 21 January 2016
Original Article

OXFORD

Original Article

Selection and characterization of Anticalins targeting human prostate-specific membrane antigen (PSMA)

Cyril Barinka[1,4,†], Jakub Ptacek[1,2,†], Antonia Richter[3], Zora Novakova[1], Volker Morath[3], and Arne Skerra[3,4]

[1]Institute of Biotechnology, Academy of Sciences of the Czech Republic, Prumyslova 595, 25242 Vestec, Czech Republic, [2]Department of Biochemistry, Faculty of Natural Science, Charles University, Albertov 6, Prague 2, Czech Republic, and [3]Munich Center for Integrated Protein Science (CIPS-M) and Lehrstuhl für Biologische Chemie, Technische Universität München, 85354 Freising (Weihenstephan), Germany

[4]To whom correspondence should be addressed. Institute of Biotechnology CAS, v.v.i., Laboratory of Structural Biology, Prumyslova 595, 25242 Vestec, Czech Republic. E-mail: cyril.barinka@ibt.cas.cz (C.B.); Lehrstuhl für Biologische Chemie, Technische Universität München, Emil-Erlenmeyer-Forum 5, 85354 Freising (Weihenstephan), Germany. E-mail: skerra@tum.de (A.S.)
[†]Equal contribution.
Edited by Anthony Rees

Received and Revised 30 November 2015; Accepted 1 December 2015

Abstract

Although prostate carcinoma (PCa) is by far the most commonly diagnosed neoplasia in men, corresponding diagnostic and therapeutic modalities have limited efficacy at present. Anticalins comprise a novel class of binding proteins based on a non-immunoglobulin scaffold that can be engineered to specifically address molecular targets of interest. Here we report the selection and characterization of Anticalins that recognize human prostate-specific membrane antigen (PSMA), a membrane-tethered metallopeptidase constituting a disease-related target for imaging and therapy of PCa as well as solid malignancies in general. We used a randomized lipocalin library based on the human lipocalin 2 (Lcn2) scaffold together with phage display and ELISA screening to select PSMA-specific variants. Five Anticalin candidates from the original panning were expressed in *Escherichia coli* as soluble monomeric proteins, revealing affinities toward PSMA down to the low nanomolar range. Binding characteristics of the most promising candidate were further improved via affinity maturation by applying error-prone PCR followed by selection via phage display as well as bacterial surface display under more stringent conditions. In BIAcore measurements, the dissociation constant of the best Anticalin was determined as ~500 pM, with a substantially improved dissociation rate compared with the first-generation candidate. Finally, immunofluorescence microscopy revealed specific staining of PSMA-positive tumor cell lines while flow cytometric analysis confirmed the ability of the selected Anticalins to detect PSMA on live cells. Taken together, Anticalins resulting from this study offer a viable alternative to antibody-based PSMA binders for biomedical applications, including *in vivo* imaging of PCa or neovasculature of solid tumors.

Key words: Anticalin, glutamate carboxypeptidase II, lipocalin, non-immunoglobulin scaffold, prostate carcinoma

Introduction

Prostate specific membrane antigen (PSMA), also known as glutamate carboxypeptidase II (GCPII) or N-acetylated-α-linked acidic dipeptidase (NAALADase), is a validated target for the *in vivo* imaging of prostate cancer (PCa) (Barinka *et al.*, 2012; Foss *et al.*, 2012). PSMA is a membrane-tethered homodimeric metallopeptidase expressed in benign prostate secretory acinar epithelium. Dysplastic and neoplastic transformation of prostate tissue is accompanied by substantial increase in PSMA expression, with the highest levels observed in high-grade, metastatic, and hormone-insensitive cancers (Wright *et al.*, 1995). Apart from PCa, increased PSMA expression has been observed also for subtypes of bladder carcinoma and Schwannoma (Wang *et al.*, 2009; Samplaski *et al.*, 2011). Furthermore, PSMA is detectable in the neovasculature of many solid tumors (Chang *et al.*, 1999; Haffner *et al.*, 2009). Therefore, bioactive molecules that target neovasculature-restricted PSMA open excellent therapeutic opportunities and offer versatile diagnostic tools for the detection of many solid cancers, in particular PCa.

Current imaging agents directed at PSMA fall into four categories, with the first two being the most advanced in the clinic: (i) antibodies, (ii) low molecular weight ligands, (iii) nanoparticles, and (iv) nucleic acid aptamers (Foss *et al.*, 2012; Mease *et al.*, 2013). At present, the only FDA-approved PSMA-specific imaging agent is a murine monoclonal antibody (mAb) radiolabeled with ^{111}In, known as ProstaScint (Ellis *et al.*, 2011). However, due to the fact that ProstaScint recognizes an intracellular epitope of PSMA it can only bind apoptotic or necrotic cells; consequently, this agent is not suitable for live cell staining, including the imaging of tumor neovasculature. This limitation was mitigated by the development of second generation mAbs which recognize extracellular epitopes of PSMA (David *et al.*, 2006; Elsässer-Beile *et al.*, 2006). The clinically most advanced agents are radiometal conjugates of the murine mAb J591 (or its humanized version) that were shown to specifically image PCa as well as other solid tumors *in vivo* (Vallabhajosula *et al.*, 2005).

Nevertheless, mAbs in general suffer from several drawbacks as imaging agents, including poor tissue penetration and long circulation times, which causes significant background radioactivity within the blood pool and non-target tissues and, consequently, poor imaging contrast (Mendler *et al.*, 2015). One of the strategies for addressing the exceptionally slow pharmacokinetics of mAb-derived imaging agents is the use of smaller aptamers or PSMA-specific low molecular weight ligands. Phosphorus- and urea-based small molecule inhibitors with (sub)nanomolar affinities are being most extensively investigated in this regard. These inhibitors typically comprise the P1' glutamate that is specifically recognized by PSMA, which is functionalized by a PET or SPECT radioisotope or an optical imaging agent. Such molecules did already prove efficacious in preclinical *in vitro* and *in vivo* models as well as in human clinical trials (Ferraris *et al.*, 2012; Foss *et al.*, 2012; Cho *et al.*, 2012; Barrett *et al.*, 2013; Nedrow-Byers *et al.*, 2013; Afshar-Oromieh *et al.*, 2014).

As an innovative strategy for the development of PSMA-specific research tools and theranostic agents we set out to design cognate Anticalins (Richter *et al.*, 2014). These engineered non-immunoglobulin binding proteins offer several benefits such as efficient expression in *E. coli*, high target specificity, good tissue penetration, and tunable plasma half-life. The Anticalin technology has been continuously developed in our laboratory during the last decade to provide a novel class of binding agents based on the human lipocalin scaffold. Lipocalins comprise a diverse family of small (20 kDa) extracellular proteins that occur in many species, ranging from bacteria to humans, and serve for the transport or scavenging of physiological compounds. Despite mutually low sequence homology, the three-dimensional fold of lipocalins is highly conserved (Schiefner and Skerra, 2015). Their single chain molecular architecture is dominated by a compact eight-stranded antiparallel β-barrel. At the open end of the barrel there are four structurally variable loops connecting each pair of β-strands. This loop region can be subjected to targeted randomization in order to yield a combinatorial Anticalin library allowing selection against a target of interest via combinatorial techniques (Gebauer and Skerra, 2012).

Several Anticalins with (sub)nanomolar affinities were successfully developed for a variety of targets (Richter *et al.*, 2014). In particular, the human lipocalin 2 (Lcn2; also referred to as NGAL, neutrophil gelatinase-associated lipocalin) led to the generation of Anticalins against well-known proteinaceous markers of human diseases:, e.g. the extra-domain B of fibronectin that is specifically expressed in neovasculature, cancer-related VEGFR-3 and Hsp70 proteins as well as the Aβ peptide implicated in Alzheimer disease and hepcidin, a negative regulator of iron homeostasis in anemia. A phase Ib clinical study with the Anticalin PRS-050 directed against VEGF-A has been successfully concluded, demonstrating Anticalins to be safe and well-tolerated while lacking anti-drug antibodies (ADAs) in humans after repeated dosing (Mross *et al.*, 2013). A phase 1 study of the Lcn2-based Anticalin PRS-080 directed against hepcidin was recently accomplished (www.pieris.com).

Taken together, Anticalins constitute a promising class of biomedical reagents that offer a valuable alternative to conventional immunoglobulins. Here we describe the selection and biochemical characterization of novel Anticalins specific for PSMA as well as the optimization of their target-binding activity *in vitro*.

Results and discussion

Preparation of PSMA variants as target proteins for selection experiments and biochemical assays

Three different versions of the extracellular region of human PSMA (residues 44–750; UniProt ID: Q04609) were constructed for this study and denoted rhPSMA, Avi-PSMA, and SF-PSMA. These differ in the presence of N-terminal fusion tags (Fig. 1): while rhPSMA shows the mature N-terminus, Avi-PSMA features the Avi-tag, which is recognized by BirA ligase that catalyzes the attachment of a single biotin group both *in vivo* and *in vitro*. Expression, purification and characterization of these two variants were previously described (Barinka *et al.*, 2002; Tykvart *et al.*, 2012).

SF-PSMA was specifically constructed for this study and comprises a TEV-cleavable N-terminal *Strep*-tag II and FLAG-tag, arranged in tandem, which allow for purification and immobilization, respectively. This variant was expressed in Schneider S2 cells and purified to homogeneity by *Strep*-Tactin affinity chromatography (Schmidt and Skerra, 2007), followed by size-exclusion chromatography (SEC). The final dimeric protein preparation was >98% pure and monodisperse, with an overall yield >5 mg/L of conditioned medium (Fig. 1).

The extracellular region of human PSMA comprises 10 potential N-glycosylation sites per monomer, all carrying an oligosaccharide chain *in vivo*. Depending on the expression host and/or tissue source, glycans can account for up to 30% of the total molecular weight of the protein (Holmes *et al.*, 1996; Barinka *et al.*, 2004a,b). Our mass-spectrometric analysis indicated that the PSMA ectodomain overexpressed in insect cells carried N-linked sugars with a combined mass of ~9.4 kDa (i.e. 12% of the polypeptide mass; data not shown).

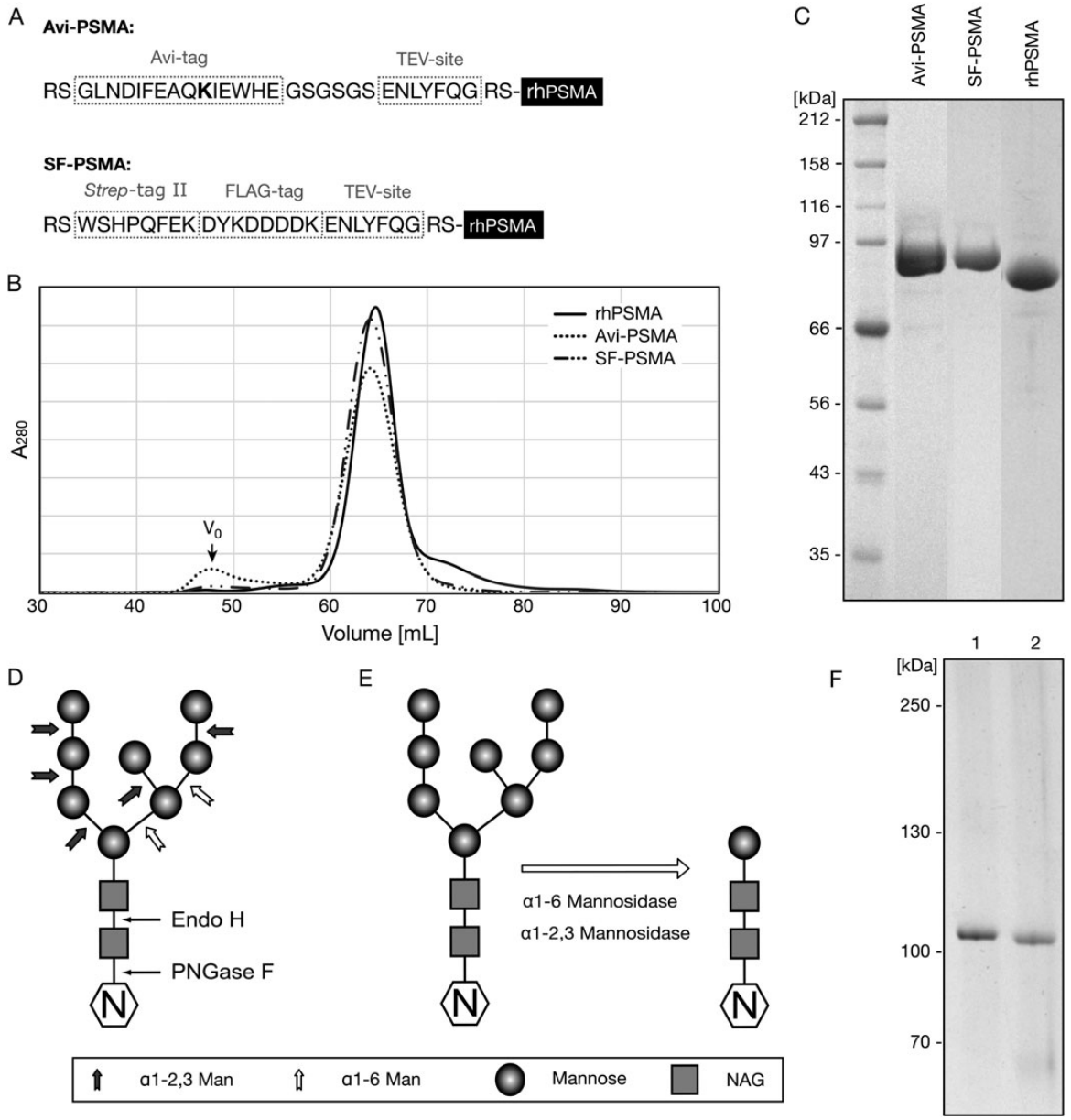

Fig. 1 PSMA variants used in this study. Three recombinant versions of the PSMA extracellular domain were produced as secreted proteins in Schneider S2 cells and purified via optimized protocols using size-exclusion chromatography (SEC) as final purification step. (**A**) Amino acid sequence at the N-terminus of the PSMA ectodomain (i.e. residues 44–750; UniProt ID: Q04609). *Avi-PSMA*: the TEV-cleavable Avi-tag is recognized *in vivo/in vitro* by BirA biotin ligase, allowing the attachment of a single biotin group at the lysine residue shown in bold. *SF-PSMA*: the cleavable N-terminal extension with the *Strep*-tag II and FLAG-tag which were employed for purification and panning, respectively. Furthermore, the wild-type ectodomain was produced with its native N-terminus (rhPSMA). (**B**) Elution profiles from a Superdex HR200 size-exclusion column documenting monodispersity of PSMA preparations. (**C**) Coomassie-stained SDS-PAGE of purified PSMA variants. Purity of all protein versions was >98%. (**D**) Specificity of endoglycosidases on a 'typical' high-mannose oligosaccharide chain attached to an N-asparagine residue of a protein. (**E**) Expected processing of N-linked sugars by the combination of α1-2,3 mannosidase and α1-6 mannosidase used in this study. (F) SDS–PAGE analysis of the fully glycosylated (lane 1) and partially deglycosylated (lane 2) SF-PSMA. Samples were resolved by SDS–PAGE using a 4–12% gradient gel (NUPAGE, Invitrogen) and silver stained.

Notably, such a high degree of N-glycosylation is likely to hamper the *in vitro* selection of binding proteins by masking/obstructing potential surface epitopes. However, it was shown that the complete removal of N-linked sugars, e.g. by PNGase F treatment or by cultivating PSMA-expressing cells in the presence of tunicamycin, leads to inactive, partially misfolded protein preparations (Barinka *et al.*, 2002; 2004a,b). To increase the accessible protein surface area of PSMA that may be targeted during Anticalin selection, while still maintaining its three-dimensional fold (as well as enzymatic activity), we used a combined treatment with α1-2,3 mannosidase and α1-6 mannosidase to partially deglycosylate the purified SF-PSMA.

This endoglycosidase processing yielded a PSMA preparation that migrated faster in SDS-PAGE, confirming the truncation of N-linked sugars (Fig. 1). At the same time, the partially deglycosylated protein retained its NAAG-hydrolyzing activity, suggesting that the overall fold of the enzyme was preserved (not shown). Both the fully

glycosylated and partially deglycosylated versions of SF-PSMA were used for the phage display panning experiments.

Selection of PSMA-specific Anticalins

The recently described 'new' Lcn2-based random library (Gebauer *et al.*, 2013) cloned on the vector pNGAL108 was used for phagemid display selection against PSMA (Fig. 2). In a first selection attempt, 100 nM Avi-PSMA was used as target for solution phase panning, i.e. Avi-PSMA/phagemid complexes were formed upon incubation and subsequently captured using Streptavidin or Neutravidin paramagnetic beads; after intense washing, the bead-bound phagemids were released by acidic elution with 0.1 M glycine/HCl, pH 2.2. Following four rounds of panning, six PSMA-reactive clones were identified via ELISA screening and subcloned for expression as soluble proteins. The resulting lipocalin variants were purified and their affinities and specificities for rhPSMA were tested. Regrettably, all variants selected by this experimental setup showed strong off-target binding as witnessed by virtually identical ELISA signals from corresponding ovalbumin-coated control plates (data not shown).

Consequently, the panning procedure was modified to increase the selectivity of elution conditions for specifically formed target/phagemid complexes by utilization of the FLAG-tagged SF-PSMA in conjunction with anti-FLAG M2 magnetic beads and competitive elution with the FLAG peptide. Additionally, the partially deglycosylated SF-PSMA (see above) was used to increase the accessibility of epitopes on the recombinant target protein. To this end, fully glycosylated and partially deglycosylated SF-PSMA were applied in a second selection campaign (cf. Scheme 1) in two parallel panning setups. 100 nM of each SF-PSMA variant was incubated with the naïve Lcn2 library and SF-PSMA/phagemid complexes were captured via the N-terminal FLAG epitope on anti-FLAG M2 magnetic beads. After intense washing, bound phagemid particles (together with the bound target protein) were competitively eluted with a 200 µg/ml solution of the FLAG peptide. Eluted phagemids were amplified in *E. coli* XL1-Blue cells and used for three successive panning cycles under the same conditions. After the fourth selection round, the pool of enriched phagemids was amplified and phasmid DNA was isolated. The *Bst*XI-flanked central lipocalin gene cassette encoding the mutagenized binding site was subcloned on the expression vector

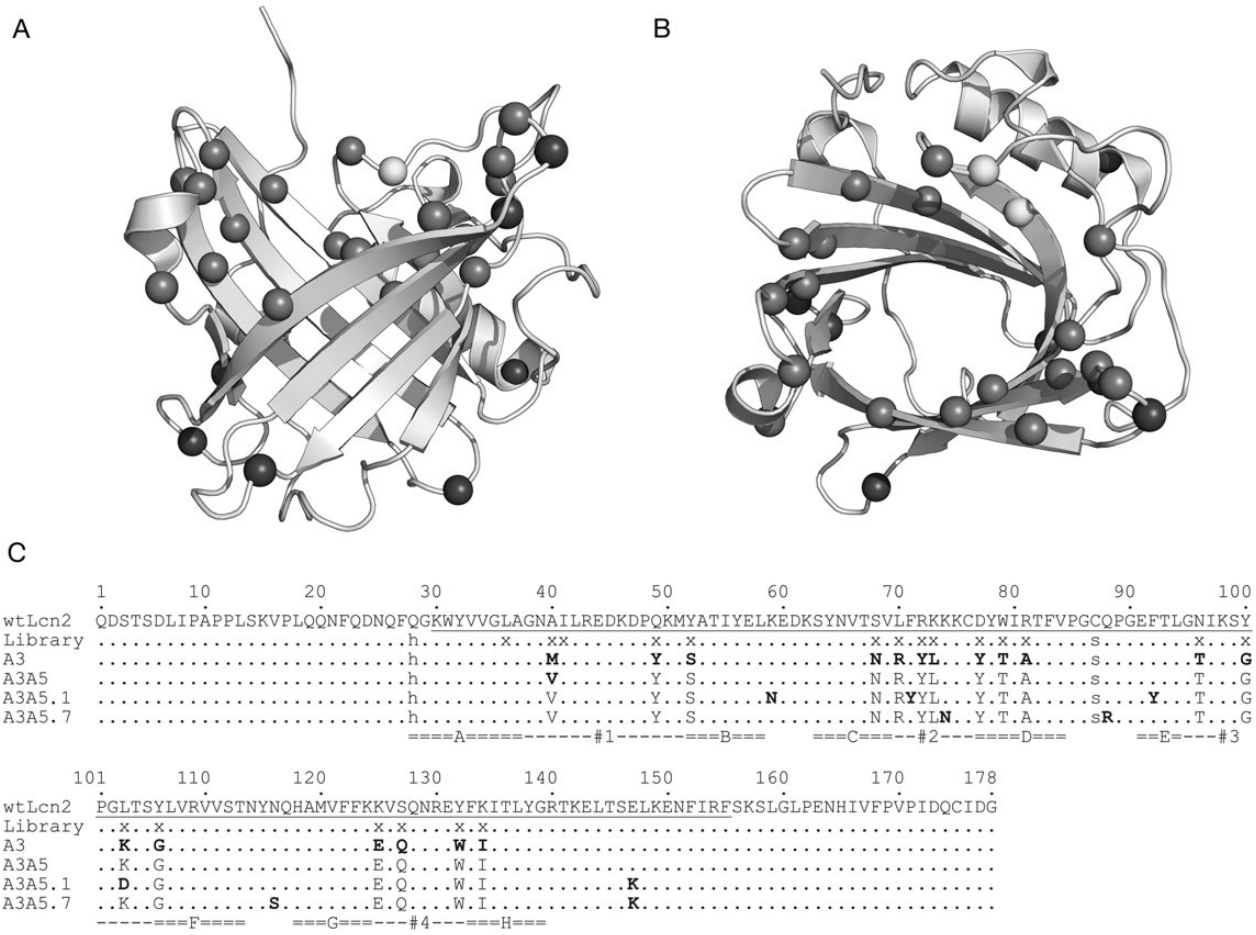

Fig. 2 3D model and sequence analysis of the selected PSMA-specific Anticalins in comparison with wild-type Lcn2. (**A, B**) Structure of human Lcn2 (PDB code: 1L6M). A rigid β-barrel composed of eight β-strands that are connected by four structurally variable loops at its open end is depicted in cartoon representation. Positions of residues that were randomized in the 'new' library are shown as white (unmutated) and grey balls. Positions in the Anticalins A3A5.1 and A3A5.7 that differ from the parent A3A5 clone are highlighted as dark grey balls. (**C**) Sequence alignment of the selected Anticalins with the template Lcn2, also illustrating the naïve Anticalin library (randomized positions denoted 'x'). A3 was selected from the original combinatorial library, while the subsequent variants emerged during affinity maturation of this clone. Positions where a given Anticalin differs from the respective parent variant are shown in bold. The central gene cassette flanked by the pair of *Bst*XI sites is underlined, β-strands and loops are labeled by letters A through H and numbers 1 through 4, respectively.

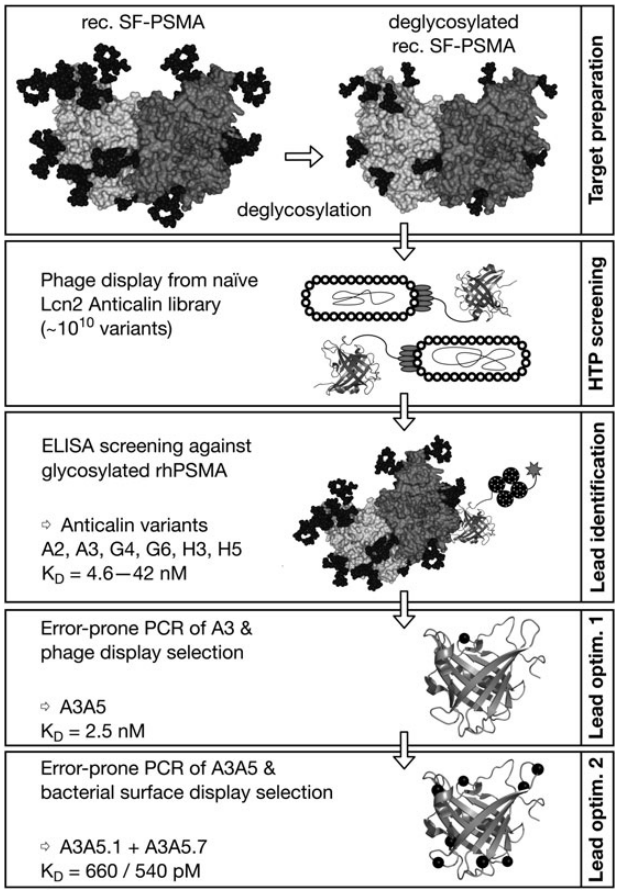

Scheme 1 Flow chart for the combinatorial selection and affinity maturation of PSMA-specific Anticalins performed in this study.

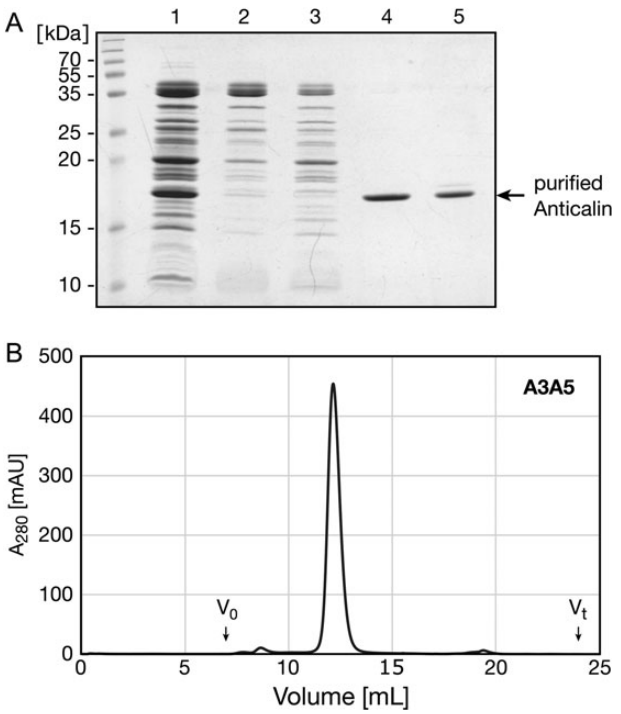

Fig. 3 Anticalin expression and purification. The selected PSMA-specific Anticalin A3A5 is shown as an example. A3A5 was produced as a soluble protein via periplasmic secretion in *E. coli* and purified by *Strep*-Tactin affinity chromatography and SEC on a Superdex HR75 column. (**A**) Coomassie-stained 15% SDS–PAGE illustrating A3A5 purification. Lanes: 1, periplasmic extract; 2, flow-through from *Strep*-Tactin column; 3, washing step; 4, elution step; 5, pooled fractions after SEC. (**B**) Elution profile from the Superdex HR75 column documents monodispersity of the A3A5 protein preparation. The elution volume corresponds to a molecular weight of 21 kDa as expected for the monomeric Anticalin. Peak fractions were pooled, concentrated and used for subsequent experiments.

pNGAL98 (Gebauer and Skerra, 2012), which allowed the production of soluble Anticalin in the periplasm of *E. coli* TG1-F$^-$.

Individual colonies were used for micro-scale expression in a 96-well plate and crude *E. coli* lysates from these cultures were screened in an ELISA for Anticalins having PSMA-binding activity. To this end, MaxiSorp plates coated with glycosylated rhPSMA were used as target, whereas ovalbumin-coated wells served as negative control to assess non-specific binding. Bound Anticalins were detected via the C-terminal *Strep*-tag II. While the first phage display selection campaign, conducted with the fully glycosylated Avi-PSMA produced in insect cells, did not yield any useful Anticalin candidates, the second attempt with the two SF-PSMA preparations was clearly successful. In total, of 172 clones that were screened 39 (~23%; 32 from the selection against partially-deglycosylated SF-PSMA, 7 from the selection against fully glycosylated SF-PSMA) gave rise to a specific signal in the ELISA.

Sequencing of these clones revealed 6 unique Anticalin candidates, of which two (denoted A2 and A3) were selected against the partially deglycosylated target and four (G4, G6, H3, and H5) were selected against the fully glycosylated target. These variants were individually produced in 2 L shake flask cultures and purified from the periplasmic cell fraction of *E. coli* via the C-terminal *Strep*-tag II and SEC. The average yield of these engineered lipocalins was in the range of 0.3–0.8 mg/L. Purity and oligomerization status were assayed by SDS–PAGE and analytical SEC, respectively, indicating that all selected variants were homogenous and monomeric with an apparent molecular weight of ~21 kDa, as expected (Fig. 3).

Biochemical characterization and affinity maturation of Anticalins

Specific binding activities of selected Anticalins toward rhPSMA as well as apparent affinity constants were initially determined by ELISA in 96-well MaxiSorp plates coated with the recombinant wild-type protein. Anticalins were applied in a dilution series and detected via the C-terminal *Strep*-tag II. Five of the six analyzed Anticalin candidates specifically recognized PSMA with apparent dissociation constants (K_D values) ranging from 6 to 42 nM, for A3 and H3, respectively (Fig. 4). For comparison, binding activity towards ovalbumin, which served as a negative control, was negligible. The G4 clone was later found to bind the anti-FLAG antibody (not shown).

The most promising variant, A3, which showed highest affinity, highest signal amplitude and low non-specific binding, was chosen for an *in vitro* affinity maturation using error-prone PCR (see Materials and Methods). First, the PCR was optimized with regard to the number of amplification cycles and template amount, aiming at the introduction of 3–6 nucleotide mutations per Anticalin gene cassette. Then, the mutated PCR fragment was subcloned via two unique and mutually non-compatible *Bst*XI sites on the plasmid pNGAL108, which allows the production of lipocalin variants in fusion with the phage minor coat protein pIII. Transformation of electrocompetent XL1-Blue cells yielded a phagemid library with a complexity of 10^8–10^9 clones and phagemid particles were produced according to published procedures (Gebauer *et al.*, 2012).

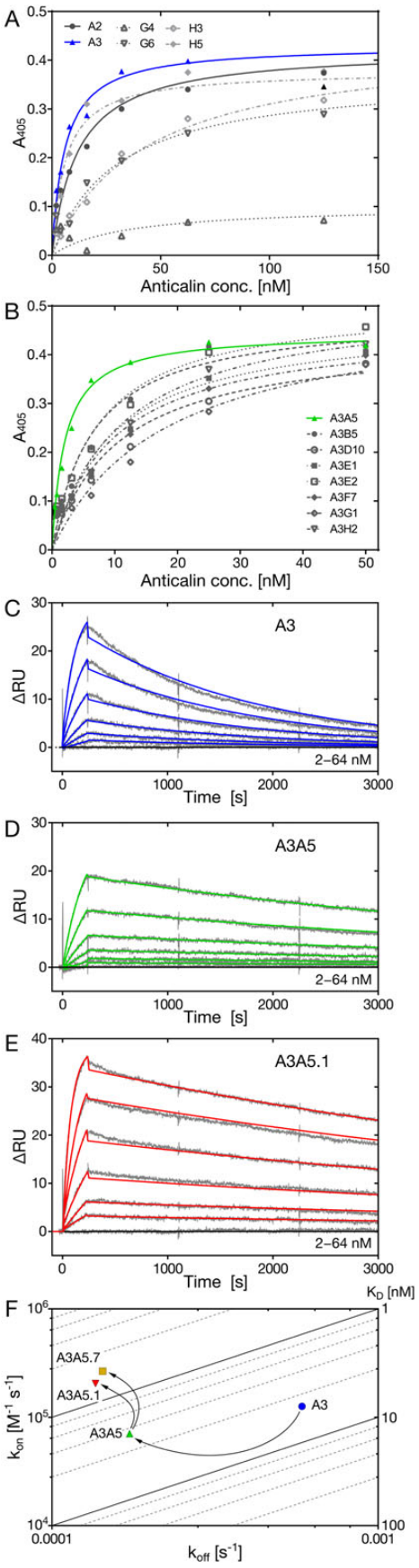

During the panning procedure, a modified setup with higher stringency was used to select for improved PSMA affinity as well as slower dissociation. To this end, a lower target concentration of 10 nM (for the first two rounds) and 1 nM (rounds 3 and 4) of Avi-PSMA was immobilized on paramagnetic beads coated with either streptavidin (rounds 1 and 3) or neutravidin (rounds 2 and 4). In this experiment the biotin-binding reagents were systematically altered to avoid selection of cognate binders. To further increase the selection pressure and avoid rebinding of dissociated phagemids, 100 nM rhPSMA was added as competitor to the first washing solution and incubated with the beads for 30 min at room temperature. After several additional washing steps with buffer, remaining bound phagemids were eluted using 100 mM glycine/HCl, pH 2.2. These phagemids were amplified, screened in an ELISA as described above, and sequenced. In total, 12 of 92 clones screened by the ELISA exhibited significantly higher signals in comparison with the original A3 clone. Among those, DNA sequencing revealed eight new clones. These were expressed at the shake flask scale, purified, and their affinities for rhPSMA were determined by ELISA (Fig. 4). The best clone, denoted A3A5, showed an apparent dissociation constant of 2.1 nM while differing from the parent A3 Anticalin by a single substitution of Val for Met at position 40 in loop #1 (cf. Fig. 2).

To search for further beneficial mutations, we applied bacterial surface display mediated by the *E. coli* autotransporter EspP, a technique previously developed for the affinity maturation of Anticalins (Binder *et al.*, 2010). To this end, the central coding region for A3A5 was subjected to another error-prone PCR as described above and subcloned on a vector that allows secretion of a fusion with the β-barrel domain of EspP and insertion into the outer membrane as well as presentation on the surface of the Gram-negative bacterium. Following incubation with Avi-PSMA and washing, cells with bound target protein were stained with a streptavidin/phycoerythrin conjugate and enriched by fluorescence-activated cell sorting (FACS). In this case, a long incubation step in the presence of an excess of the purified soluble A3A5 Anticalin, prior to washing and sorting, was used for competition and selection on slow PSMA dissociation. After four FACS cycles, two mutated Anticalin candidates were identified that showed clearly enhanced signals in single clone FACS analysis of PSMA binding: A3A5.1 and A3A5.7 (cf. Fig. 2).

Real-time affinity measurements and Anticalin-mediated detection of cellular PSMA

To precisely determine kinetic and thermodynamic binding constants of the PSMA-specific Anticalin A3 and its variants, we performed

Fig. 4 Anticalin affinities toward PSMA as determined by ELISA and BIAcore measurements. Binding activities of Anticalins selected from the original naïve library (**A**) or resulting from subsequent affinity maturation of the A3 variant (**B**) were compared in ELISA. A 96-well MaxiSorp plate was coated with rhPSMA (or ovalbumin as a negative control) and purified Anticalin variants were applied in dilution series. Anticalin binding was detected using *Strep*-Tactin/AP conjugate, followed by chromogenic reaction. Absorption was plotted against the Anticalin concentration and data were analyzed by curve fitting. Binding curves for the best performing clones A3 and A3A5 are shown in blue and green, respectively. (**C–E**) SPR sensorgrams measured for Anticalins A3, A3A5 and A3A5.1 on a BIAcore 2000 instrument. Approximately 500 RU of rhPSMA was immobilized on a CM5 sensor chip by amine coupling. A dilution series from 64 to 2 nM of the purified Anticalin in HEPES-buffered saline was applied and the resulting curves were fitted using a Langmuir 1:1 binding model. (**F**) Comparison of parameters from real-time SPR analysis for Anticalins investigated in C–E, together with A3A5.7, in a k_{on}/k_{off} plot.

Table I. Kinetic and equilibrium parameters from BIAcore analysis of PSMA-specific Anticalins

Lipocalin variant	k_{on} [10^5 M^{-1} s^{-1}]	k_{off} [10^{-4} s^{-1}]	$K_D \pm SE$ [nM]
A3	1.3	5.8	4.6 ± 0.02
A3A5	0.71	1.7	2.5 ± 0.007
A3A5.1	2.1	1.4	0.66 ± 0.0007
A3A5.7	2.7	1.4	0.54 ± 0.0005

surface plasmon resonance (SPR) real-time analyses on a BIAcore 2000 instrument. To this end, rhPSMA was chemically coupled to the carboxymethyl dextran matrix of a sensorchip using amine chemistry and a concentration series of each Anticalin was applied. As result, the initial Anticalin A3 exhibited a K_D value of 4.6 nM whereas the first mutant resulting from affinity maturation, A3A5, was two-fold improved to 2.5 nM (Table I). These results closely match the affinities of 5.8 and 2.1 nM, respectively, previously determined by ELISA. Further enhanced affinities were detected by SPR for A3A5.1 and A3A5.7, with K_D values of 660 and 540 pM, respectively.

To determine the capability of selected Anticalins to detect PSMA in its native cellular context we employed both transfected HEK293T cells and human prostate carcinoma cell lines. HEK293T cells stably transfected with a plasmid encoding full length wild-type PSMA were generated using jetPRIME transfection and Zeocin selection. In addition, the PSMA-positive and PSMA-negative prostate cancer cell lines LNCaP and PC-3, respectively, were employed. The presence/absence of human PSMA in these cell lines was confirmed by Western blotting using the mAb GCP04 that specifically recognizes PSMA (Fig. 5) (Barinka *et al.*, 2004a,b). As expected, both non-transfected HEK293T cells and the PC-3 cell line were negative for PSMA, whereas PSMA-transfected HEK293T cells as well as LNCaP cells were PSMA positive, with the HEK293T/PSMA cells expressing significantly higher levels of PSMA than LNCaP (Fig. 5A).

For immunofluorescence microscopy, the different cell lines were fixed with paraformaldehyde on glass coverslips and permeabilized. Following a blocking step, cells were probed with the Anticalin A3A5, which was detected by a murine antibody (*Strep*MAB-Immo) recognizing the *Strep*-tag II and an Alexa Fluor 488-labeled anti-mouse secondary antibody. In this manner, PSMA was stained via the Anticalin both on the plasma membrane and in the cytoplasmic region of permeabilized PSMA-positive cells, but not in the case of PSMA-negative cells (Fig. 5B). Also, when wild-type Lcn2 was used instead of the Anticalin A3A5, no fluorescent staining was detected. The intensity of the signal observed with the Anticalin for the different PSMA-positive cells was proportional to the PSMA protein level as estimated by Western blotting.

Finally, flow cytometric analysis was used to assess binding of the Anticalin A3A5 to human PSMA expressed on the surface of live PSMA-transfected HEK293T as well as LNCaP cells. Anticalin binding was again detected via indirect staining by a sandwich of *Strep*MAB-Immo and a secondary antibody labeled with Alexa Fluor 647. As seen from the flow cytometry histograms (Fig. 6), staining of PSMA-transfected HEK293T cells was stronger than for LNCaP, in line with the Western blot and immunofluorescence data. Notably, the Anticalin did not stain the two PSMA-negative control cell lines (HEK293T and PC-3), thus confirming its specificity for this target.

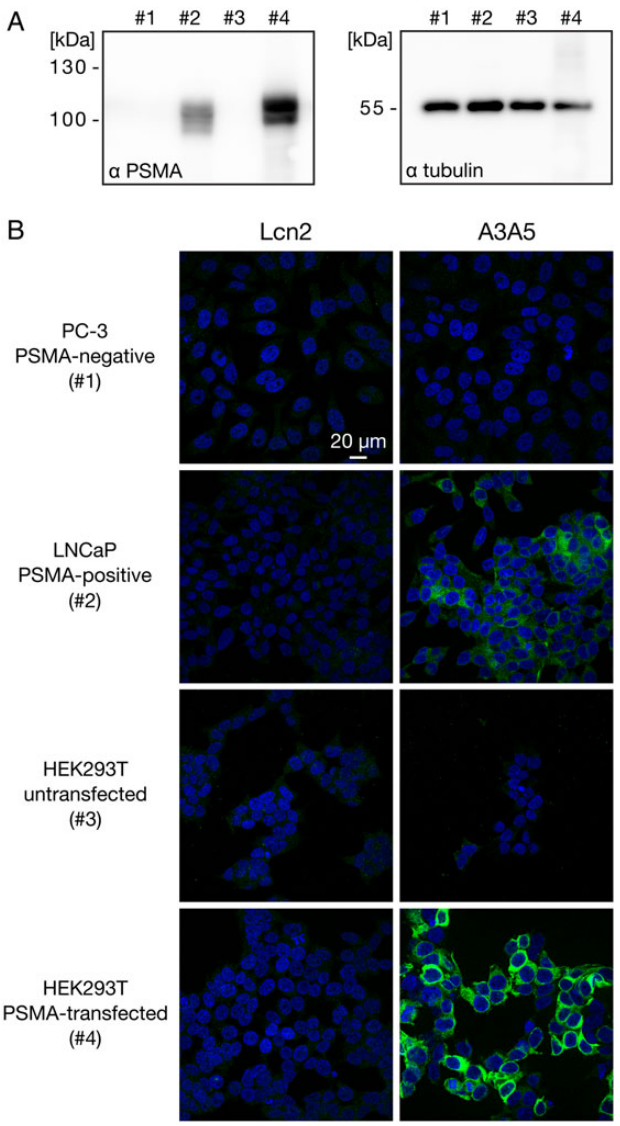

Fig. 5 Detection of PSMA expressed on cells with the Anticalin A3A5 by immunofluorescence microscopy. (**A**) Quantification of PSMA levels in cell lysates. Cell lysates were separated by 10% SDS–PAGE, transferred onto a PVDF membrane and immunostained with the antibody GCP04, followed by an anti-mouse/HRP conjugate. Expression levels were significantly higher in PSMA-transfected HEK293T cells compared to endogenously expressed PSMA in the LNCaP prostate cell line. α Tubulin was used as internal control. (**B**) PSMA-positive cell lines (LNCaP, PSMA-transfected HEK293T) and corresponding PSMA-negative controls (PC-3, HEK293T) were fixed on glass coverslips by paraformaldehyde and permeabilized. Fixed cells were probed with 0.5 µM Anticalin A3A5, followed by detection via *Strep*MAB-Immo and an Alexa Fluor 488-labeled anti-mouse secondary antibody. Both plasma membrane and cytoplasmic staining is detectable for PSMA-positive LNCaP and, even more pronounced, PSMA-transfected HEK293T cells. PSMA-negative PC-3 prostate cell line and non-transfected HEK293T cells revealed no staining. Nuclei were visualized with DAPI.

Conclusions

A recently published comprehensive validation of immunohistochemical biomarkers of prostate cancer showed that PSMA – beside AKT1, stromal androgen receptor, and EZH2 – is one of only four independently prognostic markers for prostate-specific antigen (PSA) relapse following radical prostatectomy (Huber *et al.*, 2015). Together with the fact that PSMA is being evaluated as a 'universal' marker for the neovasculature of solid tumors, this membrane-anchored enzyme represents an attractive target for biomedical cancer research. Anticalins with their compact size offer an interesting

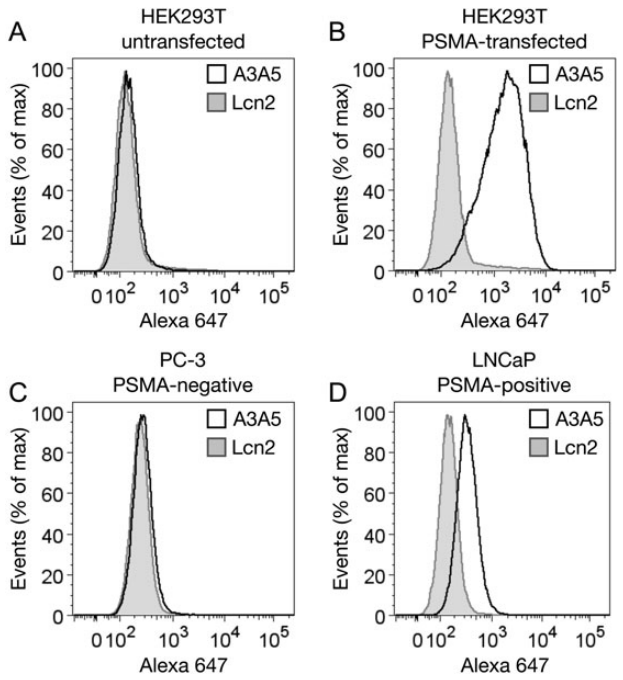

Fig. 6 Flow cytometry analysis of PSMA expression on live cells. Two cell lines of prostate origin, LNCaP (PSMA$^+$, **D**) and PC-3 (PSMA$^-$, **C**), along with PSMA-transfected HEK293T cells (**B**; with the matching non-transfected HEK293T included as control, **A**) were used to assess binding of the Anticalin (1 μM) to PSMA in its native environment on the surface of live cells. Bound Anticalin was detected with *Strep*MAB-Immo and a secondary anti-mouse antibody labeled with Alexa Fluor 647. Open (black line) histograms show the staining profile for the Anticalin A3A5 while filled (grey) histograms indicate the background fluorescence intensity measured for wild-type Lcn2. A3A5 staining intensity was weaker for LNCaP cells due to lower amounts of PSMA present at the cell surface, in agreement with Western blotting and immunofluorescence data (cf. Fig. 5). A minimum of 20 000 cells were analyzed for each sample using FlowJo software.

alternative to traditional antibody-based reagents. Showing a pharmacokinetic profile more similar to that of small molecules, which is preferred in clinical practice, they exhibit high target specificity similar to mAbs. This study demonstrates that Anticalins provide novel and promising PSMA-specific reagents that recognize this tumor target protein in its native conformation and, consequently, appear attractive for the development of imaging agents for prostate cancer or even as drug-targeting vehicles for therapy.

Materials and methods

Expression and purification of human PSMA variants

Three variants of human PSMA featuring different N-terminal tags were used throughout this study (Fig. 1) and produced as secreted proteins in Schneider S2 cells. The conditioned media (SFX serum-free medium; ThermoFisher Scientific) was concentrated, dialyzed by tangential flow filtration (TFF; Millipore), and target proteins were purified according to optimized protocols as detailed in the following.

Wild-type rhPSMA

Cloning, expression and purification of the extracellular part of human PSMA (rhPSMA; denoted rhGCPII in the original paper, residues 44–750) were carried out as described (Barinka *et al.*, 2002). The protein was purified using ion-exchange chromatography (Q and SP Sepharose FF), affinity chromatography on Lentil-Lectin Sepharose, and size-exclusion chromatography (SEC) on a Superdex 16/60 HR200 column with 20 mM Tris/HCl, 150 mM NaCl, pH 8.0 as mobile phase (all resins/columns from GE Healthcare). Purified rhPSMA was concentrated to 1 mg/ml and kept frozen at −80°C until further use.

Avi-PSMA

The extracellular part of human PSMA comprising an N-terminal Avi-tag (Avi-PSMA) was prepared as previously described (Tykvart *et al.*, 2012). Briefly, the recombinant protein was expressed in Schneider S2 cells stably transfected with *E. coli* biotin protein ligase localized to the endoplasmic reticulum. After coexpression of the fusion protein, single-step purification was carried out on a resin carrying an immobilized streptavidin mutant (Streptavidin Mutein Matrix, Roche) with biotin elution. SEC as above yielded the final preparation with >95% purity. Avi-PSMA was aliquoted, shock-frozen in liquid nitrogen and stored at −80°C until further use.

SF-PSMA

A *Strep*-FLAG-TEV sequence (Fig. 1A) was introduced at the N-terminus of the coding region for the extracellular part of human PSMA (residues 44–750) by polymerase chain reaction (PCR). The PCR product was cloned via *Bgl*II and *Xho*I restriction sites on pMT/BiP/V5-His A (Invitrogen) resulting in the plasmid pMT/BiP/SF-PSMA. This plasmid, together with pCoBLAST which confers resistance to blasticidine (InvivoGen), was transfected into Schneider S2 cells using Effectene (Qiagen) according to the manufacturer's protocol. Two days post transfection, transfectants were selected by adding 50 μg/ml blasticidine into the serum-free SFX medium supplemented with 10% v/v fetal bovine serum (FBS). Approximately three weeks post transfection, the blasticidine-resistant S2 cell population was transferred into SFX medium, expanded, and expression of SF-PSMA was induced by the addition of 0.7 mM $CuSO_4$ at a cell density of 1×10^6/ml. Seven days post induction, $\sim 30 \times 10^6$ cells per ml were harvested by centrifugation and the conditioned medium was concentrated by tangential flow filtration to 1/10 of the original volume. Concentrated medium was dialyzed three times against at least 10-fold excess of 50 mM Tris/HCl, 150 mM NaCl, pH 8.0 (TBS). Dialyzed medium was loaded onto a 5 ml *Strep*-Tactin column (IBA) equilibrated in TBS and the SF-PSMA protein was eluted with 3 mM D-desthiobiotin (IBA) in TBS. Pooled elution fractions containing pure SF-PSMA were concentrated and loaded onto a Superdex 16/60 HR200 size-exclusion column equilibrated in TBS. Fractions corresponding to the SF-PSMA dimer were pooled, concentrated to 1 mg/ml by ultrafiltration, snap-frozen in liquid nitrogen and stored at −80°C until further use. The typical yield of SF-PSMA was about 5 mg per liter culture with purity >99% (Fig. 1).

For partial deglycosylation, SF-PSMA (10 μg) was mixed with both α1-2,3 mannosidase (64 U) and α1-6 mannosidase (80 U; both from New England Biolabs) in a volume of 50 μl. The deglycosylation reaction was carried out at 37°C for 4 h and monitored by SDS–PAGE.

Selection of Anticalins against PSMA via phage display

The 'new' Lcn2 library (Gebauer *et al.*, 2013) served as a starting point for the selection of PSMA-specific Anticalins. In this library, twenty specified amino acid positions within the structurally variable loops and adjoining segments around the natural ligand pocket were randomized to generate a genetic library amenable for phage display

selection of lipocalin variants with prescribed binding activities. This Anticalin library was encoded on the pNGAL108 plasmid in frame with the N-terminal OmpA signal peptide and the C-terminal *Strep*-tag II, followed by the pIII minor coat protein of bacteriophage M13 (Gebauer and Skerra, 2012).

The successful selection of PSMA-specific lipocalin variants from the naïve library was carried out by on-bead panning essentially following a published procedure (Gebauer and Skerra, 2012). To this end, 100 nM SF-PSMA was first incubated with 10^{11} phagemids of the library in TBS + 2% w/v BSA in a total volume of 500 µl for 1 h at room temperature. SF-PSMA/phagemid complexes were then captured for 10 min using 25 µl of Anti-FLAG M2 magnetic beads (Sigma-Aldrich). Following magnetic separation, unbound phagemids were discarded and the beads were washed ten times with TBS containing 0.1% v/v Tween-20 (TBS/T; 0.5 ml per washing step). Finally, bound phagemid/SF-PSMA complexes were released from the beads by competitive elution with an excess of the FLAG peptide (300 µl of 200 µg/ml; Sigma-Aldrich) in TBS/T. Amplification of eluted phagemids was performed as described (Gebauer and Skerra, 2012). A total of four panning cycles were carried out in this way using 10^9–10^{11} phagemids from the preceding panning round as input. The phasmid DNA of the enriched population from the last cycle was isolated with the Qiagen Plasmid Midiprep Kit (Qiagen) and subjected to subcloning on the plasmid pNGAL98 for soluble expression and ELISA screening (see below).

For affinity maturation via phage display, the panning procedure was modified as follows: instead of SF-PSMA, Avi-PSMA was incubated with the blocked phagemid library in solution and Avi-PSMA/phagemid complexes were captured via Streptavidin magnetic beads (50 µl; Roche; rounds 1 and 3) or Neutravidin-coated Sera-Mag Speed beads (50 µl; Thermo Scientific; rounds 2 and 4) in an alternating manner. 10 nM Avi-PSMA target was used for the first two rounds whereas the concentration was decreased to 1 nM in rounds 3 and 4. Bead-bound phagemids were washed under more stringent conditions with first TBS/T containing 0.1 mM D-desthiobiotin as well as 100 nM rhPSMA for 30 min (to select for slow k_{off}), followed by nine washing steps with TBS/T + desthiobiotin for 1 min. Bound phagemids were finally released by acidic elution with 350 µl of 0.1 M glycine/HCl pH 2.2 for 10 min and immediately neutralized by addition of 55 µl 0.5 M Tris base (pH 10.5).

Affinity maturation via phage display

A second generation Anticalin library was generated by error-prone PCR based on the Anticalin A3 template obtained from the original anti-PSMA selection campaign using the GeneMorph II random mutagenesis kit (Agilent Technologies). First, the Anticalin gene was amplified from the pNGAL98 expression vector by *Taq* DNA polymerase using the primers 5′-AGA CAG CTA TCG CGA TTG CA and 5′-CGC AGT AGC GGT AAA CG. The amplified DNA fragment was purified from an agarose gel with the QIAquick Gel Extraction Kit (Qiagen) and used as template for the error-prone PCR, which was carried out according to the manufacturer's protocol. Shortly, 1 ng of the template together with the primers *Bst*XI-for (5′-CAG GAC AAC CAA TTC CAT GGG) and *Bst*XI-rev (5′-GGA GGC CCA GAG ATT TGG) that flank the central region of the Anticalin gene, comprising all four previously randomized loop segments, were used to introduce an optimal number of 4–6 nucleotide mutations per gene during a total of 30 reaction cycles. The resulting PCR product was purified from agarose gel and ligated with the phage display vector pNGAL108 using *Bst*XI restriction sites, followed by electroporation of *E. coli* XL1-Blue cells as described (Gebauer and Skerra, 2012). The complexity of the resulting sublibrary was assessed by plating a dilution series of transformed cells and revealed typically about 10^8–10^9 individual clones. Finally, phagemid particles were produced and used for the panning rounds as described above.

Identification of PSMA-specific Anticalin candidates by high-throughput ELISA

Enriched lipocalin variants from phage display were subjected to ELISA screening after subcloning of the central *Bst*XI gene cassette on pNGAL98, which also encodes the N-terminal OmpA signal sequence directing the expressed protein into the bacterial periplasm and a C-terminal *Strep*-tag II for purification (Schmidt and Skerra, 2007). After transformation of *E. coli* TG1-F$^-$ (Kim *et al.*, 2009) with the ligation mixture, randomly picked colonies were inoculated in a 96-well plate filled with 100 µl of Terrific broth (TB) medium supplemented with 100 µg/ml ampicillin (Amp) per well. Anticalin expression was induced at an optical density OD_{550} = 0.3–0.5 by addition of 20 µl TB/Amp containing 1.2 µg/ml anhydrotetracycline (aTc; ACROS Organics) overnight at 20°C. The periplasmic extract was prepared as previously described (Gebauer and Skerra, 2012) and applied to 96-well MaxiSorp plates (Nunc) coated with rhPSMA (5 µg/ml in TBS) and blocked with BSA. Ovalbumin (10 µg/ml in TBS) served as non-related control protein in parallel. After 1 h incubation at room temperature, plates were washed three times with phosphate-buffered saline supplemented with 0.1% v/v Tween-20 (PBS/T) and bound lipocalin variants were detected by means of their C-terminal *Strep*-tag II using *Strep*-Tactin conjugated to alkaline phosphatase (IBA), diluted 1:5000 in PBS, for 1 h. Signals were developed using 0.5 mg/ml *p*-nitrophenyl phosphate in 0.1 M NaCl, 5 mM $MgCl_2$, 0.1 M Tris/HCl, pH 8.8, and monitored via absorbance measurement at 405 nm with an Infinite 200 PRO microplate reader (Tecan).

Affinity maturation via bacterial surface display

First, a library based on the Lcn2 variant A3A5 was constructed via error-prone PCR as described above. The resulting PCR product was digested with *Bst*XI, purified and ligated with the plasmid pNGAL146 (Gebauer and Skerra, 2012), which encodes a fusion protein between the lipocalin and the β-domain of the bacterial autotransporter EspP. The resulting Anticalin library was used for transformation of electro-competent *E. coli* JK321 cells (Jose *et al.*, 1996), followed by plating on Luria-Bertani (LB)/Amp agar.

Bacterial cultivation, target incubation, staining and fluorescence-activated cell sorting (FACS) were carried out as described before (Binder *et al.*, 2010). In brief, colonies were scraped from the agar plate, suspended in 50 ml LB/Amp medium and shaken for 1 h at 37°C. This culture was used to inoculate a 50 ml LB/Amp overnight culture at 30°C which in turn was used the next day to inoculate 50 ml LB/Amp at 30°C with a starting OD_{550} = 0.15. Gene expression was induced at OD_{550} = 0.5 with 10 ng/ml aTc for 2.5 h. Cells from 100–200 µl of this culture were spun down in an Eppendorf tube for 3 min at 4°C, washed once in PBS with 3% w/v BSA (PBS/BSA) and resuspended in 1000 µl PBS/BSA supplemented with 2.5 or 1 nM Avi-PSMA (see below). After 1 h incubation under gentle shaking at 4°C the cells were washed and incubated in the presence of 100 nM purified A3A5 Anticalin as competing PSMA ligand. After that, cells were washed once and remaining bound Avi-PSMA was

stained by subsequent incubation with PBS/BSA containing 25 µg/ml streptavidin/phycoerythrin (SA/PE; BD Biosciences) and 3 µM DY634-labelled A3C5 Fab fragment directed against a peptide tag as part of the Anticalin-autotransporter fusion protein (Binder *et al.*, 2010). Following 30 min incubation on ice the cells were finally washed once with PBS and then applied to a FACSAria cell-sorting system (BD Biosciences).

For fluorescence detection of PE, a 488 nm laser diode and a 530/30 band pass filter was used, while DY634 was detected using a HeNe laser (633 nm) and a 660/20 band pass filter. In each of the four selection rounds the fraction comprising the 0.3–0.5% most fluorescent cells were sorted and propagated for the next cycle. The stringency of selection was gradually increased by lowering the concentration of Avi-PSMA (2.5 nM in rounds 1 and 2; 1 nM in rounds 3 and 4) and increasing the duration of the competitive dissociation step from 3 h in round 1 to 30 h in round 4. Finally, single clones were analyzed by DNA sequencing of the *Bst*XI gene cassette as well as individual cultivation, staining and single-clone FACS analysis. For further analysis of promising candidates, the *Bst*XI gene cassette was subcloned on pNGAL98 as above.

Anticalin expression and purification

Anticalin candidates were produced via periplasmic secretion in *E. coli* using the vector pNGAL98 in shake flasks according to a standard procedure (Gebauer and Skerra, 2012). Transformed *E. coli* TG1-F$^-$ were cultured in LB/Amp medium at 22°C and 180 rpm until exponential growth was reached. Then, expression was induced for 3 h by addition of aTc to a final concentration of 200 µg/L. Bacteria were harvested by centrifugation and the periplasmic extract was prepared by a mild osmotic shock and subsequent removal of spheroplasts by centrifugation. The recombinant Anticalins were purified by means of *Strep*-Tactin affinity chromatography (Schmidt and Skerra, 2007), followed by SEC on a Superdex 16/60 HR75 column equilibrated in PBS.

Anticalin affinity measurement by ELISA

50 µl of rhPSMA (5 µg/ml in TBS) was directly adsorbed onto the surface of a MaxiSorp 96-well plate overnight at 4°C. Similarly, ovalbumin-coated wells (10 µg/ml in PBS) were used as a negative control. After blocking with BSA for 1 h at room temperature, 50 µl from a serial Anticalin dilution in PBS was added to each well and incubated for 1 h. The plates were washed three times and bound Anticalins were detected with *Strep*-Tactin/AP as described further above. The data were analyzed using Prism 5 software (GraphPad) and absorption values (A) were fitted according to the formula $\Delta A = A_{max} \cdot [L_{tot}]/(K_D + [L_{tot}])$ with the concentration of the applied lipocalin variant $[L_{tot}]$ and the dissociation constant K_D.

BIAcore real-time affinity measurements

SPR spectroscopy was performed on a BIAcore 2000 instrument following published procedures (De Crescenzo *et al.*, 2008; Gebauer *et al.*, 2013). rhPSMA (1 nM in 10 mM Na-acetate pH 5.0) was immobilized on a CM5 sensor chip (BIAcore) using an amine coupling kit (GE Healthcare), resulting in around 500 resonance units (ΔRU). The purified Anticalins were diluted in HEPES-buffered saline (HBS; 10 mM HEPES/NaOH, 150 mM NaCl, pH 7.4) with 0.005% v/v Tween-20 to concentrations from 64 to 2 nM. The instrument was operated using the same running buffer at a flow rate of 25 µl/min. Complex formation was monitored by injection of 100 µl of the Anticalin solution and dissociation was observed for 100 min. Regeneration of the sensor chip was achieved by up to four injections of 10 µl glycine/HCl, pH 2.0. The sensorgrams were corrected by double subtraction of the corresponding signals measured for the in-line control channel and an averaged baseline determined from three buffer blank injections (Myszka, 1999). Kinetic parameters were determined by data fitting using a 1:1 Langmuir binding model with BIAevaluation software version 4.1 (BIAcore).

Cell lines

The PSMA-positive LNCaP (provided by Z. Hodny, IMG, Prague, Czech Republic) and PSMA-negative PC-3 (provided by M. Pomper, JHMI, Baltimore, MD) prostate carcinoma cell lines were grown in RPMI-1640 medium (Sigma-Aldrich) supplemented with 10% v/v FBS. The HEK293T/17 cell line was purchased from the American Type Culture Collection (CRL-11268) and grown in Dulbecco's modified Eagle's medium in the presence of 10% v/v FBS under a humidified 5% CO_2 atmosphere at 37°C. HEK293T/17 cells overexpressing PSMA were generated by jetPRIME-mediated transfection (Polyplus-transfection) using the vector pcDNA4/V5-His A (Invitrogen) carrying the nucleotide sequence for full-length human PSMA (FOLH1; NM_004476.1). The PSMA-expressing clone was obtained by repeated cloning of a single cell under selection pressure of Zeocin (25 µg/ml; InvivoGen).

Western blotting and immunodetection

PSMA-overexpressing cells were washed with PBS, collected by centrifugation and lysed in 50 mM Tris/HCl pH 6.8, 2% w/v SDS, 10% v/v glycerol. The total protein concentration in the cell lysate was estimated using the BCA protein assay (Pierce Biotechnology), and 20 µg of protein per lane were loaded on a 10% SDS polyacrylamide gel. After electrophoresis, proteins were transferred onto a PVDF membrane (Millipore) and PSMA was detected by subsequent incubation with the GCP04 primary antibody (Barinka *et al.*, 2004a,b) and an anti-mouse secondary antibody conjugated to horseradish peroxidase (Bio-Rad), followed by signal development with Luminata Forte chemiluminescence substrate (Millipore). Signals were recorded with an ImageQuant LAS 4000 imager (GE Healthcare) and processed with Adobe Photoshop software.

Immunofluorescence microscopy

PSMA-positive and -negative cells grown on cover slides coated with gelatin (0.1% w/v) were washed twice with PBS, fixed with 4% w/v paraformaldehyde in PBS for 15 min, permeabilized by treatment with PBS containing 0.1% v/v Triton X-100 for 15 min, and incubated in the blocking solution (5% w/v non-fat dried milk in PBS) for 30 min at room temperature. Cells were then incubated with 0.5 µM Anticalin in blocking solution for 45 min followed by incubation with the *Strep*-tag II specific monoclonal antibody *Strep*MAB-Immo (2 µg/ml in PBS containing 0.05% v/v Tween-20; IBA) for 1 h. Finally, an anti-mouse secondary antibody conjugated to Alexa Fluor 488 (5 µg/ml; Life Technologies) was applied for 1 h. All incubation steps were interspersed by extensive washing with PBS containing 0.05% v/v Tween-20. Processed slides were treated with 4′,6-diamidino-2-phenylindole (DAPI; 1 µg/ml; Sigma) for 5 min, mounted in VectaShield medium (Vector Laboratories) and imaged with a TCS SP5 confocal microscope equipped with a 63× immersion oil objective (Leica Microsystems). Images were processed using Adobe Photoshop software.

Flow cytometry

Cells were detached by PBS supplemented with 0.25% w/v trypsin and 0.02% w/v EDTA, washed, centrifuged, resuspended in PBS containing 2% w/v BSA and incubated with 1 μM purified Anticalin for 30 min at 4°C in a total volume of 20 μl. Next, the cell suspension was incubated with the *Strep*MAB-Immo antibody (6.7 μg/ml) for 30 min at 4°C in a total volume of 40 μl. Finally, cells were incubated with an anti-mouse secondary antibody conjugated to Alexa Fluor 647 (4 μg/ml; Life Technologies) for 30 min at 4°C in a total volume of 50 μl. All incubations and washing steps were performed in PBS containing 2% w/v BSA. To label dead cells, Hoechst 33258 was added to the samples immediately before flow cytometric analysis. Cells were analyzed using an LSRII flow cytometer (BD Biosciences) and data were processed using FlowJo software. Only viable cells (negative for Hoechst staining) were analyzed.

Acknowledgements

We thank Petra Baranova (Institute of Biotechnology, Vestec) for the excellent technical assistance.

Funding

This work was supported by the Czech Science Foundation (grant No 301/12/1513), the project 'BIOCEV' (CZ.1.05/1.1.00/02.0109) from the ERDF, the Deutsche Forschungsgemeinschaft, Germany, with the Collaborative Research Centre SFB 824, and the Federal State of Bavaria and the Deutsche Forschungsgemeinschaft in frame of their Major Research Instrumentation Programme (Grant No. INST 95/1031-1). J.P. acknowledges support from GAUK (grant no. 510112) and C.B. acknowledges a short-term EMBO travel fellowship (contract No. ATSF-56-2012).

References

Afshar-Oromieh,A., Avtzi,E., Giesel,F.L., *et al.* (2014) *Eur. J. Nucl. Med. Mol. Imaging*, **42**, 197–209.

Barinka,C., Rinnova,M., Sacha,P., Rojas,C., Majer,P., Slusher,B.S. and Konvalinka,J. (2002) *J. Neurochem.*, **80**, 477–487.

Barinka,C., Mlcochova,P., Sacha,P., Hilgert,I., Majer,P., Slusher,B.S., Horejsi, V. and Konvalinka,J. (2004a) *Eur. J. Biochem.*, **271**, 2782–2790.

Barinka,C., Sacha,P., Sklenar,J., Man,P., Bezouska,K., Slusher,B.S. and Konvalinka,J. (2004b) *Protein Sci.*, **13**, 1627–1635.

Barinka,C., Rojas,C., Slusher,B. and Pomper,M. (2012) *Curr. Med. Chem.*, **19**, 856–870.

Barrett,J.A., Coleman,R.E., Goldsmith,S.J., *et al.* (2013) *J. Nucl. Med.*, **54**, 380–387.

Binder,U., Matschiner,G., Theobald,I. and Skerra,A. (2010) *J. Mol. Biol.*, **400**, 783–802.

Chang,S.S., Reuter,V.E., Heston,W.D., Bander,N.H., Grauer,L.S. and Gaudin, P.B. (1999) *Cancer Res.*, **59**, 3192–3198.

Cho,S.Y., Gage,K.L., Mease,R.C., *et al.* (2012) *J. Nucl. Med.*, **53**, 1883–1891.

David,K.A., Milowsky,M.I., Kostakoglu,L., Vallabhajosula,S., Goldsmith,S.J., Nanus,D.M. and Bander,N.H. (2006) *Clin. Genitourin Cancer*, **4**, 249–256.

De Crescenzo,G., Woodward,L. and Srinivasan,B. (2008) *J. Mol. Recognit.*, **21**, 256–266.

Ellis,R.J., Kaminsky,D.A., Zhou,E.H., Fu,P., Chen,W.D., Brelin,A., Faulhaber,P.F. and Bodner,D. (2011) *Int. J. Radiat. Oncol. Biol. Phys.*, **81**, 29–34.

Elsässer-Beile,U., Wolf,P., Gierschner,D., Bühler,P., Schultze-Seemann,W. and Wetterauer,U. (2006) *Prostate*, **66**, 1359–1370.

Ferraris,D.V., Shukla,K. and Tsukamoto,T. (2012) *Curr. Med. Chem.*, **19**, 1282–1294.

Foss,C.A., Mease,R.C., Cho,S.Y., Kim,H.J. and Pomper,M.G. (2012) *Curr. Med. Chem.*, **19**, 1346–1359.

Gebauer,M. and Skerra,A. (2012) *Methods Enzymol.*, **503**, 157–188.

Gebauer,M., Schiefner,A., Matschiner,G. and Skerra,A. (2013) *J. Mol. Biol.*, **425**, 780–802.

Haffner,M.C., Kronberger,I.E., Ross,J.S., *et al.* (2009) *Hum. Pathol.*, **40**, 1754–1761.

Holmes,E.H., Greene,T.G., Tino,W.T., Boynton,A.L., Aldape,H.C., Misrock,S. L. and Murphy,G.P. (1996) *Prostate Suppl.*, **7**, 25–29.

Huber,F., Montani,M., Sulser,T., *et al.* (2015) *Br. J. Cancer*, **112**, 140–148.

Jose,J., Kramer,J., Klauser,T., Pohlner,J. and Meyer,T.F. (1996) *Gene*, **178**, 107–110.

Kim,H.J., Eichinger,A. and Skerra,A. (2009) *J. Am. Chem. Soc.*, **131**, 3565–3576.

Mease,R.C., Foss,C.A. and Pomper,M.G. (2013) *Curr. Top. Med. Chem.*, **13**, 951–962.

Mendler,C.T., Friedrich,L., Laitinen,I., Schlapschy,M., Schwaiger,M., Wester, H.J. and Skerra,A. (2015) *MAbs*, **7**, 96–109.

Mross,K., Richly,H., Fischer,R., Scharr,D., Buchert,M., Stern,A., Gille,H., Audoly,L.P. and Scheulen,M.E. (2013) *PLoS One*, **8**, e83232.

Myszka,D.G. (1999) *J. Mol. Recognit.*, **12**, 279–284.

Nedrow-Byers,J.R., Moore,A.L., Ganguly,T., Hopkins,M.R., Fulton,M.D., Benny,P.D. and Berkman,C.E. (2013) *Prostate*, **73**, 355–362.

Richter,A., Eggenstein,E. and Skerra,A. (2014) *FEBS Lett.*, **588**, 213–218.

Samplaski,M.K., Heston,W., Elson,P., Magi-Galluzzi,C. and Hansel,D.E. (2011) *Mod. Pathol.*, **24**, 1521–1529.

Schiefner,A. and Skerra,A. (2015) *Acc. Chem. Res.*, **48**, 976–985.

Schmidt,T.G. and Skerra,A. (2007) *Nat. Protoc.*, **2**, 1528–1535.

Tykvart,J., Sacha,P., Barinka,C., Knedlik,T., Starkova,J., Lubkowski,J. and Konvalinka,J. (2012) *Protein Expr. Purif.*, **82**, 106–115.

Vallabhajosula,S., Kuji,I., Hamacher,K.A., *et al.* (2005) *J. Nucl. Med.*, **46**, 634–641.

Wang,W., Tavora,F., Sharma,R., Eisenberger,M. and Netto,G.J. (2009) *Urol. Oncol.*, **27**, 525–528.

Wright,G.L., Jr., Haley,C., Beckett,M.L. and Schellhammer,P.F. (1995) *Urol. Oncol.*, **1**, 18–28.